Chemical Science

ROYAL SOCIETY OF CHEMISTRY

EDGE ARTICLE

View Article Online
View Journal | View Issue

Cite this: *Chem. Sci.*, 2023, **14**, 8564

All publication charges for this article have been paid for by the Royal Society of Chemistry

Received 2nd June 2023
Accepted 13th July 2023

DOI: 10.1039/d3sc02800c

rsc.li/chemical-science

Rhodium-catalyzed annulative approach to N–N axially chiral biaryls *via* C–H activation and dynamic kinetic transformation†

Xiaohan Zhu,[a] Hongli Wu,[b] Yishou Wang,[c] Genping Huang, *[b] Fen Wang*[a] and Xingwei Li [ac]

N–N axially chiral biaryls represent a rarely explored class of atropisomeric compounds. We hereby report rhodium-catalyzed enantioselective [4 + 2] oxidative annulation of internal alkynes with benzamides bearing two classes of N–N directing groups. The coupling occurs under mild conditions *via* NH and CH annulation through the dynamic kinetic transformation of the directing group and is highly enantioselective with good functional tolerance. Computational studies of a coupling system at the DFT level has been conducted, and the alkyne insertion was identified as the enantio-determining as well as the turnover-limiting step.

Introduction

Axially chiral compounds have received considerable attention in the past decades owing to their wide presence in natural products and pharmaceuticals and extensive applications as chiral ligands or oganocatalysts.[1] To date, the vast majority of the studies have been limited to those containing a C–C or C–N axis, and catalytic atroposelective synthesis of such molecules has been extensively investigated (Scheme 1a).[2] In stark contrast, catalytic asymmetric construction of N–N atropisomers lags far behind,[3] although N–N axial chirality is widely present in diverse biologically active molecules,[4] natural products,[5] ligands,[6] and functional materials.[7] For example, the schischkinii was isolated as a natural product from the seeds of *Centaurea schischkinii*.[4b] Moreover, the indoloterpenoid dixiamycins A and B have been identified as a pair of N–N atropisomers.[5b,c] Furthermore, 2,2′-bis(diphenylphosphanyl)-1,1′-bibenzimidazole (BIMIP) has been employed as a useful chiral bisphosphine ligand.[6] In addition, DOBCz has been applied as an organic light-emitting diodes material.[7] Therefore, the development of catalytic asymmetric methods to construct N–N axially chiral biaryls is under increasing demand.

Three synthetic strategies have been developed toward asymmetric construction of chiral axis, namely, desymmetrization, NH-functionalization or NH_2-difunctionalization, and peripheral C–H functionalization. In 2021, the group of Lu and Liu reported an enantioselective synthesis of bisindoles through Cu-catalyzed desymmetrizative Friedel–Crafts alkylation of symmetrical bisindoles (Scheme 1b left).[8] Lu and Houk developed an original quinidine-catalyzed *N*-allylation of an amino group, accomplishing the 1st asymmetric construction of N–N axially chiral indoles (Scheme 1b middle).[9] Shortly

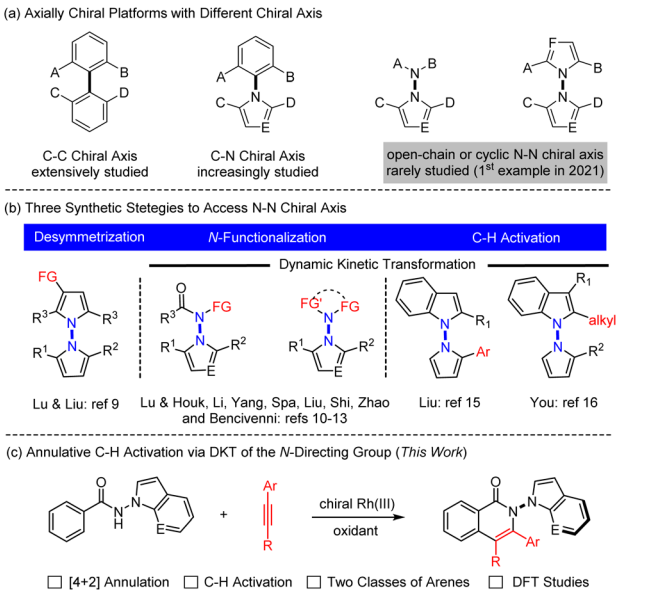

Scheme 1 Representative atropisomers and enantioselective construction of N–N biaryl atropisomers.

[a]*School of Chemistry and Chemical Engineering, Shaanxi Normal University, Xi'an 710062, China. E-mail: fenwang@snnu.edu.cn*

[b]*Department of Chemistry, School of Science and Tianjin Key Laboratory of Molecular Optoelectronic Sciences, Tianjin University, Tianjin 300072, China. E-mail: gphuang@tju.edu.cn*

[c]*Institute of Molecular Science and Engineering, Institute of Frontier and Interdisciplinary Sciences, Shandong University, Qingdao 266237, China*

† Electronic supplementary information (ESI) available. CCDC 2213499. For ESI and crystallographic data in CIF or other electronic format see DOI: https://doi.org/10.1039/d3sc02800c

afterwards, increasing reports have documented metal- or organocatalyzed *N*–NH functionalization by virtue of dynamic kinetic transformations.[10] Analogously, organocatalyzed [4 + 1] annulative difunctionalization of a *N*–NH_2 group also provided an alternative avenue to access chiral indole-based biaryls in high enantioselectivity (Scheme 1b middle), as have been recently independently disclosed by Shi,[11] Zhao,[12] and Liu.[13]

Alternatively, C–H bond activation has emerged as a powerful strategy to access C–C and C–N axially chiral biaryls.[14] In 2023, the Liu[15] and You[16] groups realized independent synthesis of N–N biaryl atropisomers through dynamic kinetic transformation (DKT) of indoles or pyrroles *via* palladium- or iridium-catalyzed enantioselective C–H functionalization (Scheme 1b, right). Despite the versatility of asymmetric C–H activation in construction of new chiral platforms,[17] its applications toward construction of N–N axially chiral framework remain largely underdeveloped. In addition, the existing few examples (Scheme 1b, right) are also limited to simple, single-site C–H functionalization of indole rings that are intrinsically reactive.[15,16] As a continuation of our ongoing interest in asymmetric synthesis of non-indole-based biaryl atropisomers *via* C–H functionalization,[18] we now report [4 + 2] annulative coupling of readily available benzamides bearing different *N*-directing groups, where both proximal C–H and NH bonds are functionalized to give N–N axially chiral 5,6-biaryls in high enantioselectivity (Scheme 1c). Of note, the redox-neutral [4 + 2] annulation *via* N–N cleavage has been fully suppressed.

Results and discussion

We commenced our exploration with optimization studies on the [4 + 2] annulation between benzamide **1** and diphenylacetylene (**2**) in the presence of a chiral CpXRh(III) catalyst (Table 1). It was found that the employment of **(*R*)-Rh1** (3 mol%) as a catalyst in the presence of PivOH (2.0 equiv.) and Ag_2O (2.0 equiv.) in MeOH at 30 °C afforded the desired product (**3**) in high enantioselectivity (88% ee) but with a low yield (entry 1). Further screening of solvents indicated that toluene was superior in terms of reaction efficiency, albeit with slightly lower enantioselectivity (entries 2–3). A series of chiral catalysts were then explored, and the **(*R*)-Rh6** outperformed the rest in terms of both activity and stereoselectivity (entries 7–11), under which conditions good high and excellent enantioselectivity (−96% ee) have been secured (entry 11). In this case, the oppositely configured product **3** was obtained due to opposite spatial orientation of the chiral ligand in **(*R*)-Rh6** despite the same nomenclature. The amount of the oxidant and additive were examined. However, reducing the amount of Ag_2O and $MesCO_2H$ essentially had marginal effect on the efficiency and enantioselectivity (entry 13, Conditions A). Finally, switching the oxidant to other silver(I) oxidants only give lower efficiency or enantioselectivity (entries 14–16).

With the optimal conditions in hand, the scope of the *N*-indolyl benzamide substrates was next examined (Scheme 2). The presence of alkyl and halogen groups at the 3- or 6-position in indole ring was tolerated, affording the desired products in good yield and excellent enantioselectivity (**3–6**, −94 to −96% ee) under the standard reaction conditions. Of note, the **(*R*)-Rh1** catalyst could also catalyze this reaction in the presence of a mixed silver salt oxidants (entry 6, in Table 1, Conditions B) in high yield and excellent enantioselectivity (**(*ent*)-3**, 94% ee), whose absolute configuration has been determined by X-ray crystallography (CCDC 2213499). However, the Conditions B suffered from compatibility issues with various substrates (see comparisons of these two conditions for synthesis of **12** and **14**). Therefore, the standard Conditions A in Table 1 (entry 13) were employed in most of our studies. Under these conditions, the presence of diverse *meta* and *para* substituents in the benzene ring were also well tolerated (**7–9**). An *ortho* substituent in the benzamide did not compromise the enantioselectivity but influenced the reaction efficiency and caused a decrease in yield (**10**). Symmetric diarylacetylenes bearing a range of electron-donating, electron-withdrawing, and halogen groups at *para* position were fully compatible, affording products **11–15** in excellent enantioselectivity. In addition to symmetric alkynes, some unsymmetrical alkynes could also react to give the desired products (**16–18**) with excellent regioselectivity under modified conditions. 1,3-Enynes with an alkyl or phenyl terminal group underwent [4 + 2] annulations with the benzamide, furnishing the desired products **19** and **20** in moderate yields and high enantioselectivities. Extension of the *N*-group to *N*-dihydroquinolinone also gave product **21** with a 6,6-heterocyle linkage in excellent enantioselectivity and low yield. In contrast, poor reactivity (<5% yield) was observed for the coupling of 3-hexyne under either conditions A or B (Scheme 2).

To better explore the applicability of arene substrates, we next moved to benzamides bearing a *N*-azaindolyl group (**22**, Scheme 3). It was found that the modified catalytic conditions of **(*R*)-Rh-1** (3 mol%)/$AgSbF_6$ (12 mol%), AgOAc (2.0 equiv.) and AcOH (1.0 equiv.) allowed the formation of the desired product **23** in a high isolated yield (87%) and excellent enantioselectivity (94% ee) with DCE being a solvent. The absolute configuration of product **23** has been determined by ECD spectroscopy and confirmed by DFT studies. Thus, benzamides with a large array of methyl, methoxy, trifluoromethyl, and halogen substituents at different positions of the benzene ring were all compatible (**23–29**, 94–98% ee), with no significant electronic effect being observed on the enantioselectivity. In particular, a 3-thiophenecarboxamide also reacted smoothly in this reaction system (**30**, 92% ee). The scope of internal alkynes **2** was next examined. Symmetrical diarylalkynes bearing electron-donating (methyl and *tert*-butyl) and -withdrawing (trifluoromethyl and bromide) groups at the *para* position were well compatible, and the corresponding products **32–35** were delivered in high yields (87–93%) with excellent enantioselectivities (90–92% ee). *meta*-(Di)substituted alkynes also reacted smoothly to afford the corresponding product **36** and **37** in excellent stereoselectivity. Moreover, when a hereroaromatic alkyne was used, the product **38** was obtained in moderate yield and excellent enantioselectivity (92% ee). In addition, for a nonsymmetric alkyne, the corresponding product **39** was obtained only with moderate yield and enantioselectivity (75% ee). To understand the conformational stability of such N–N axial atropisomers, racemization studies have been conducted for

Table 1 Optimization of the reaction condition[a]

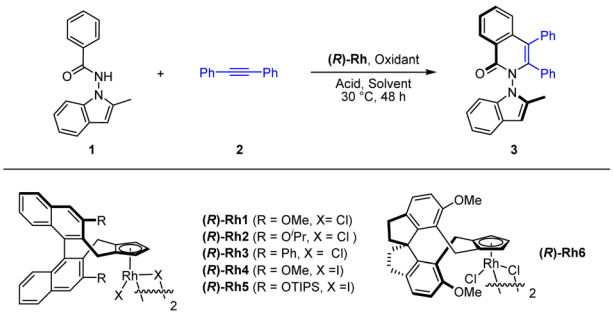

Entry	Rh cat.	Oxidant (equiv.)	Acid (equiv.)	Solvent	ee (%)	Yield (%)
1	**(*R*)-Rh1**	Ag_2O (2.0)	HOPiv (2.0)	MeOH	88	32
2	**(*R*)-Rh1**	Ag_2O (2.0)	HOPiv (2.0)	DCE	72	34
3	**(*R*)-Rh1**	Ag_2O (2.0)	HOPiv (2.0)	PhMe	84	49
4	**(*R*)-Rh1**	Ag_2O (2.0)	$MesCO_2H$ (2.0)	PhMe	88	55
5	**(*R*)-Rh1**	Ag_2CO_3 (2.0)	$MesCO_2H$ (2.0)	PhMe	98	39
6[b]	**(*R*)-Rh1**	Ag_2O (1.0) Ag_2CO_3 (0.5)	$MesCO_2H$ (2.0)	PhMe	94	70
7	**(*R*)-Rh2**	Ag_2O (2.0)	$MesCO_2H$ (2.0)	PhMe	94	45
8	**(*R*)-Rh3**	Ag_2O (2.0)	$MesCO_2H$ (2.0)	PhMe	—	<5
9	**(*R*)-Rh4**	Ag_2O (2.0)	$MesCO_2H$ (2.0)	PhMe	91	50
10	**(*R*)-Rh5**	Ag_2O (2.0)	$MesCO_2H$ (2.0)	PhMe	—	<5
11	**(*R*)-Rh6**	Ag_2O (2.0)	$MesCO_2H$ (2.0)	PhMe	−96	67
12	**(R)-Rh6**	Ag_2O (1.5)	$MesCO_2H$ (2.0)	PhMe	−95	67
13	**(*R*)-Rh6**	**Ag_2O (1.5)**	**$MesCO_2H$ (1.2)**	**PhMe**	**−96**	**68**
14	**(*R*)-Rh6**	Ag_2CO_3 (1.5)	$MesCO_2H$ (1.2)	PhMe	−97	40
15	**(*R*)-Rh6**	AgF (1.5)	$MesCO_2H$ (1.2)	PhMe	−84	43
16	**(*R*)-Rh6**	AgOAc (1.5)	$MesCO_2H$ (1.2)	PhMe	—	<5

[a] Reaction conditions: **1** (0.1 mmol), **2** (0.15 mmol), **(*R*)-Rh** catalyst (3 mol%), oxidant (2.0 equiv.), and an acid (2.0 equiv.) in a solvent (2 mL), 30 °C, 48 h. [b] 60 °C. Isolated yield. The ee was determined by HPLC analysis using a chiral stationary phase.

a representative product **23** at 120 °C in mesitylene (see ESI†). The rotational barrier of **23** was estimated to be 32.8 kcal mol^{-1}, indicating the high atropoisomeric stability of this N–N axis. Additionally, scale-up synthesis of **23** (1 mmol) was successful, with essentially no decay of enantiopurity.

Representative products have been studied toward further synthetic or catalytic transformations as given in Scheme 4. Treatment of product **(*ent*)-3** with NBS afforded the 3-brominated product in excellent yield (**40**). Ru(II)-catalyzed oxidative olefination of product **(*ent*)-3** with styrene gave product **41** in essentially the same optical purity. Treatment of **23** with I_2O_5 led to selective iodination at the *N*-azaindole ring (**42**). The pyridine ring in a related axially chiral product **23** offers synthetic handles. *m*-CPBA oxidation of **23** afforded the *N*-oxide (**43**) in high yield. Further reaction with *para*-bromotoluene under palladium catalysis delivered the arylated product **44**. We next applied *N*-oxide **43** as a chiral ligand in Pd-catalyzed insertion of an *N*-protected indole into a donor–acceptor carbene reagent, affording the alkylated product **45** in promising enantioselectivity (59% ee).

To gain a better understanding of the detailed reaction mechanism and factors that contribute to enantioselectivity, DFT calculations were performed at the $M06_{(SMD)}$/def2-TZVPP//B3LYP-D3(BJ)/def2-SVP level of theory (see the ESI† for the computational details). The experimentally used benzamide **1** and diphenylacetylene **2** were selected as the model substrates in the computations (Fig. 1). The calculated energy profile of the most favorable pathway leading to [4 + 2] oxidative annulation product (S_{NN})-**3** is given in Fig. 1. Starting from active catalyst species **CAT** derived from the **(*R*)-Rh-1** catalyst, the N–H deprotonation gives the intermediate (S_{NN})-**IM1**, which was calculated to be endergonic by 5.9 kcal mol^{-1}. The ensuing C–H bond cleavage occurs *via* the well-established concerted metallation deprotonation (CMD) mechanism[19] through transition state (S_{NN})-**TS1**, with an energy barrier of 22.2 kcal mol^{-1} relative to **CAT**. The resulted five-membered rhodacycle intermediate (S_{NN})-**IM2** was found to be more stable than (S_{NN})-**IM1** by 6.1 kcal mol^{-1}. The computations indicate that the alkyne insertion into the Rh–C bond directly from (S_{NN})-**IM2** is kinetically unfavorable (see the ESI† for details). Instead, an isomerization step involving the rotation of Rh–Cp bond[20] must occur first to give intermediate (S_{NN})-**IM3**. Subsequently, the alkyne insertion into the Rh–C bond proceeds *via* transition state (S_{NN})-**TS2**, leading to seven-membered rhodacycle species (S_{NN})-**IM4**. This intermediate then undergoes the C–N reductive elimination *via* transition state (S_{NN})-**TS3** to forge product-coordinated intermediate (S_{NN})-**IM4**, from which product (S_{NN})-**3** can be obtained by the re-oxidation of Rh

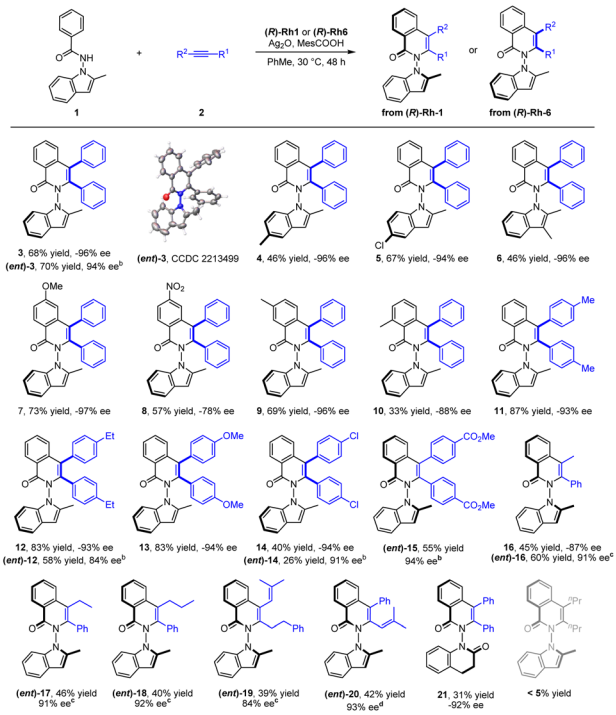

Scheme 2 Scope of *N*-indolyl benzamides **1** as substrates for the synthesis of N–N atropisomers. (a) Reaction conditions A: **1** (0.1 mmol), **2** (0.15 mmol), **(*R*)-Rh6** (3 mol%), Ag_2O (1.5 equiv.), and MesCOOH (1.2 equiv.) in toluene (2 mL), 30 °C, 48 h. Isolated yield. The ee was determined by HPLC analysis using a chiral stationary phase. (b) Reaction conditions B: **1** (0.1 mmol), **2** (0.15 mmol), **(*R*)-Rh1** (3 mol%), Ag_2O (1.0 equiv.), Ag_2CO_3 (0.5 equiv.) and MesCOOH (2.0 equiv.) in toluene (2 mL), 60 °C, 48 h. (c) Reaction conditions C: **1** (0.1 mmol), **2** (0.15 mmol), **(*R*)-Rh1** (3 mol%), Ag_2CO_3 (1.0 equiv.), Ag_2O (0.5 equiv.), and HOPiv (2.0 equiv.) in toluene (2 mL), 30 °C, 48 h. (d) Reaction conditions D: **1** (0.1 mmol), **2** (0.15 mmol), **(*R*)-Rh1** (3 mol%), Ag_2O (2.0 equiv.), and HOPiv (2.0 equiv.) in toluene (2 mL), 30 °C, 48 h.

center to regenerate active catalyst species **CAT** with the assistance of oxidant AgOAc.

The computations show that the alkyne insertion into the Rh–C bond constitutes the rate- and enantioselectivity determining step of the overall reaction.[21] This is also consistent with the poor chiral control during the C–H activation step (cyclometallation). To pinpoint the origin of the enantioselectivity, the pathway leading to product (R_{NN})-**3** was also considered (see the ESI† for the whole calculated energy profile). The calculated energy difference of 2.1 kcal mol^{-1} between enantiomeric insertion transition states (S_{NN})-**TS2** and (R_{NN})-**TS2** corresponds to a predicted enantioselectivity of 92% ee at the reaction temperature (25.5 *versus* 27.6 kcal mol^{-1}, Fig. 2), which agrees very well with experimentally-observed 94% ee. The optimized geometries imply that the relative orientation of the alkyne is quite different in (S_{NN})-**TS2** and (R_{NN})-**TS2** (Fig. 2). Specifically, the alkyne is positioned to the right side of the benzamide moiety in (S_{NN})-**TS2** so that the five-membered rhodacycle intermediate can readily undergo the insertion process without notable geometric change. In contrast, in (R_{NN})-**TS2** the alkyne was located to the left side of the benzamide moiety. As a result,

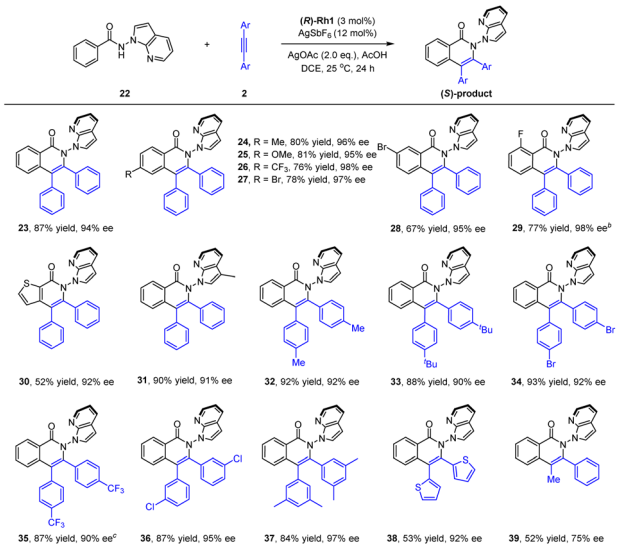

Scheme 3 Scope of *N*-azaindolyl benzamides as substrates for the synthesis of N–N atropisomers. (a) Reaction conditions: **1** (0.1 mmol), **2** (0.1 mmol), **(*R*)-Rh1** (3 mol%), $AgSbF_6$ (12 mol%), AgOAc (2.0 equiv.), AcOH (1.0 equiv.) in DCE (1 mL), 24 h, isolated yield. The ee was determined by HPLC using a chiral stationary phase. (b) 50 °C. (c) 25 °C, 60 h.

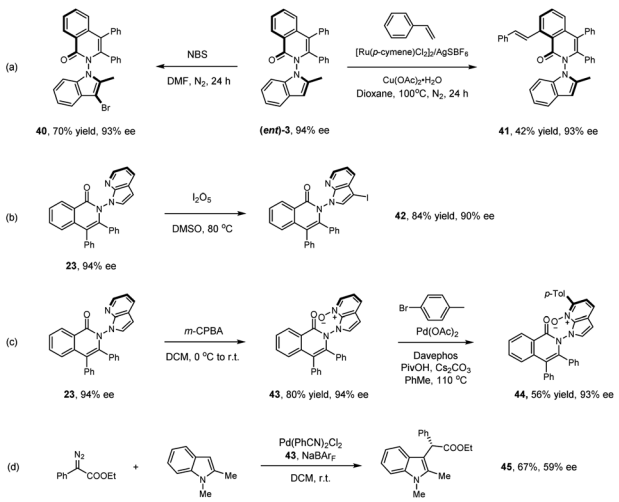

Scheme 4 Versatile synthetic transformation of representative N–N axially chiral products.

to proceed the insertion process, the five-membered rhodacycle intermediate must undergo significant distortion to create a vacant side for the incoming alkyne, resulting in (R_{NN})-**TS2** higher in energy than (S_{NN})-**TS2**. It should be mentioned that the insertion transition state (R_{NN})-**TS2′**, wherein the relative orientation of the alkyne is the same as in (S_{NN})-**TS2**, was also evaluated, but it was calculated to be 3.3 kcal mol^{-1} higher in energy than (S_{NN})-**TS2** (*i.e.*, 1.2 kcal mol^{-1} higher in energy than (R_{NN})-**TS2**). This is likely due to that the steric repulsion between the benzamide moiety and the chiral cyclopentadienyl ligand in (R_{NN})-**TS2′** is greater than that in (S_{NN})-**TS2** (see the ESI† for

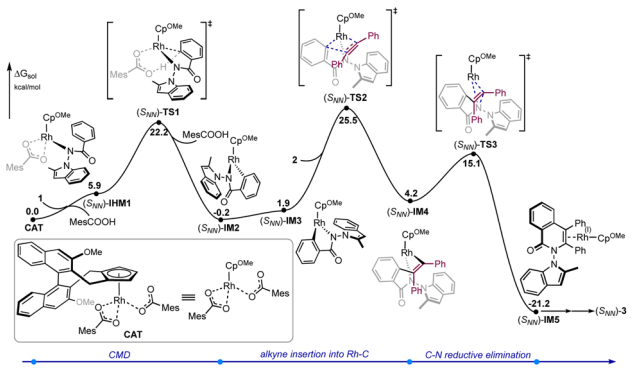

Fig. 1 Calculated energy profiles of rhodium-catalyzed enantioselective [4 + 2] oxidative annulation of diphenylacetylene **2** with benzamide **1**.

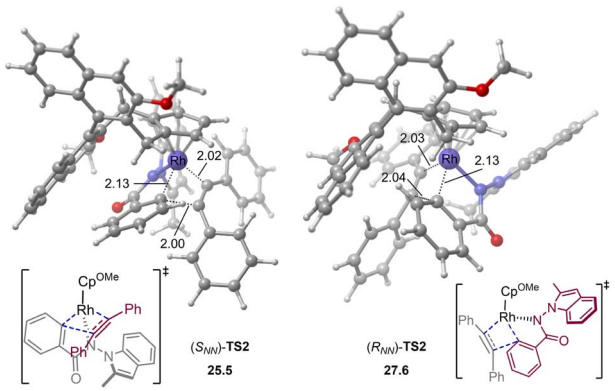

Fig. 2 Optimized geometries of alkyne insertion transition states. Energies and bond distances are given in kcal mol^{-1} and Å, respectively.

details). Therefore, the steric repulsion results in the change of the mode of the alkyne insertion, enabling the experimentally-observed enantioselectivity. In addition, our computational free energy profile is also in good agreement with our experimentally observed kinetic isotope effect (KIE = 2.3, see ESI†). The C–H activation event (22.2 kcal mol^{-1}) contributes a considerable portion to the overall kinetic barrier (25.5 kcal mol^{-1}).

Conclusions

In conclusion, we have developed two classes of asymmetric [4 + 2] annulative functionalization reactions of alkynes with benzamides bearing different types of N–N directing groups. The reaction proceeds *via* dynamic kinetic transformation (DKT) of the directing group through Rh^{III}-catalyzed C–H activation, which afforded a series of N–N axially chiral biaryls in high yields and excellent atroposelectivities. The reaction of benzamides bearing *N*-indolyl group and alkynes afforded *N*-quinolinoneindoles. By using benzamides with an *N*-azaindole ring as arene substrates, we precisely demonstrated assembly of N–N atropisomers. DFT calculations provided insight into the reaction mechanism and the enantioselective control. The strategy of *de novo* construction of a N–N chiral axis is currently explored toward precise synthesis of related axially chiral biaryls in our laboratory.

Data availability

Further details of the experimental procedure, ^{1}H, and ^{13}C NMR, HPLC spectra, and X-ray crystallographic data for **(*ent*)-3** and DFT calculations are available in the ESI.†

Author contributions

X. Z. and Y. W. performed experiments. G.-P. H. performed DFT calculations. F. W., G.-P. H. and X. L. conceived and directed the project and wrote the paper. All authors discussed the results and commented on the manuscript.

Conflicts of interest

The authors declare no competing financial interests.

Acknowledgements

We acknowledge the financial support for this work from the NSFC (22101167 and 22073066) and the Shaanxi Normal University.

Notes and references

1 For a review: (*a*) G. Bringmann, T. Gulder, T. A. M. Gulder and M. Breuning, *Chem. Rev.*, 2011, **111**, 563–639; (*b*) S. Erbas-Cakmak, D. A. Leigh, C. T. McTernan and A. L. Nussbaumer, *Chem. Rev.*, 2015, **115**, 10081–10206; (*c*) E. Kumarasamy, R. Raghunathan, M. P. Sibi and J. Sivaguru, *Chem. Rev.*, 2015, **115**, 11239–11300; (*d*) J. E. Smyth, N. M. Butler and P. A. Keller, *Nat. Prod. Rep.*, 2015, **32**, 1562–1583; (*e*) S. T. Toenjes and J. L. Gustafson, *Future Med. Chem.*, 2018, **10**, 409–422; (*f*) S. Perreault, J. Chandrasekhar and L. Patel, *Acc. Chem. Res.*, 2022, **55**, 2581–2593; (*g*) M. Basilaia, M. H. Chen, J. Secka and J. L. Gustafson, *Acc. Chem. Res.*, 2022, **55**, 2904–2919.

2 For selected reviews, see: (*a*) G. Bringmann, A. J. P. Mortimer, P. A. Keller, M. J. Gresser, J. Garner and M. Breuning, *Angew. Chem., Int. Ed.*, 2005, **44**, 5384–5427; (*b*) J. Wencel-Delord, A. Panossian, F. R. Leroux and F. Colobert, *Chem. Soc. Rev.*, 2015, **44**, 3418–3430; (*c*) Y.-B. Wang and B. Tan, *Acc. Chem. Res.*, 2018, **51**, 534–547; (*d*) B. Zilate, A. Castrogiovanni and C. Sparr, *ACS Catal.*, 2018, **8**, 2981–2988; (*e*) H. Yang, J. Chen and L. Zhou, *Chem.–Asian J.*, 2020, **15**, 2939–2951; (*f*) V. Corti and G. Bertuzzi, *Synthesis*, 2020, **52**, 2450–2468; (*g*) D.-J. Cheng and Y.-D. Shao, *Adv. Synth. Catal.*, 2020, **362**, 3081–3099; (*h*) Y.-C. Zhang, F. Jiang and F. Shi, *Acc. Chem. Res.*, 2020, **53**, 425–446; (*i*) J. A. Carmona, C. Rodríguez-Franco, R. Fernández, V. Hornillos and J. M. Lassaletta, *Chem. Soc. Rev.*, 2021, **50**, 2968–2983; (*j*) O. Kitagawa, *Acc. Chem. Res.*, 2021, **54**, 719–730; (*k*)

B.-M. Yang, X. Q. Ng and Yu Zhao, *Chem Catalysis*, 2022, **2**, 3048–3076.

3 G. Centonze, C. Portolani, P. Righi and G. Bencivenni, *Angew. Chem., Int. Ed.*, 2023, e3138202303966.

4 (*a*) J. T. Klein, L. Davis, G. E. Olsen, G. S. Wong, F. P. Huger, C. P. Smith, W. W. Petko, M. Cornfeldt, J. C. Wilker, R. D. Blitzer, E. Landau, V. Haroutunian, L. L. Martin and R. C. Effland, *J. Med. Chem.*, 1996, **39**, 570–581; (*b*) K. Suzuki, I. Nomura, M. Ninomiya, K. Tanaka and M. Koketsu, *Bioorg. Med. Chem. Lett.*, 2018, **28**, 2976–2978.

5 (*a*) M. Shoeb, S. Celik, M. Jaspars, Y. Kumarasamy, S. M. MacManus, L. Nahar, P. K. Thoo-Lin and S. D. Sarker, *Tetrahedron*, 2005, **61**, 9001–9006; (*b*) Q. Zhang, A. Mándi, S. Li, Y. Chen, W. Zhang, X. Tian, H. Zhang, H. Li, W. Zhang, S. Zhang, J. Ju, T. Kurtán and C. Zhang, *Eur. J. Org. Chem.*, 2012, 5256–5262; (*c*) Z. Xu, M. Baunach, L. Ding and C. Hertweck, *Angew. Chem., Int. Ed.*, 2012, **51**, 10293–10297.

6 T. Benincori, E. Brenna, F. Sannicolò, L. Trimarco, P. Antognazza, E. Cesarotti, F. Demartin, T. Pilati and G. Zotti, *J. Organomet. Chem.*, 1997, **529**, 445–453.

7 X.-Y. Liu, Y.-L. Zhang, X. Fei, L.-S. Liao and J. Fan, *Chem.–Eur. J.*, 2019, **25**, 4501–4508.

8 X.-M. Wang, P. Zhang, Q. Xu, C.-Q. Guo, D.-B. Zhang, C.-J. Lu and R.-R. Liu, *J. Am. Chem. Soc.*, 2021, **143**, 15005–15010.

9 (*a*) G.-J. Mei, J. J. Wong, W. Zheng, A. A. Nangia, K. N. Houk and Y. Lu, *Chem*, 2021, **7**, 2743–2757; (*b*) Q. Xu, H. Zhang, F.-B. Ge, X.-M. Wang, P. Zhang, C.-J. Lu and R.-R. Liu, *Org. Lett.*, 2022, **24**, 3138–3143.

10 (*a*) M. Pan, Y.-B. Shao, Q. Zhao and X. Li, *Org. Lett.*, 2022, **24**, 374–378; (*b*) W. Lin, Q. Zhao, Y. Li, M. Pan, C. Yang, G.-H. Yang and X. Li, *Chem. Sci.*, 2022, **13**, 141–148; (*c*) C. Portolani, G. Centonze, S. Luciani, A. Pellegrini, P. Righi, A. Mazzanti, A. Ciogli, A. Sorato and G. Bencivenni, *Angew. Chem., Int. Ed.*, 2022, **61**, e202209895; (*d*) V. Hutskalova and C. Sparr, *Synthesis*, 2023, **55**, 1770–1782; (*e*) L.-Y. Wang, J. Miao, Y. Zhao and B.-M. Yang, *Org. Lett.*, 2023, **25**, 1553–1557.

11 K.-W. Chen, Z.-H. Chen, S. Yang, S.-F. Wu, Y.-C. Zhang and F. Shi, *Angew., Chem. Int. Ed.*, 2022, **61**, e202116829.

12 Y. Gao, L.-Y. Wang, T. Zhang, B.-M. Yang and Y. Zhao, *Angew. Chem. Int., Ed.*, 2022, **61**, e202200371.

13 P. Zhang, Q. Xu, X.-M. Wang, J. Feng, C.-J. Lu, Y. Li and R.-R. Liu, *Angew. Chem., Int. Ed.*, 2022, **61**, e202212101.

14 (*a*) G. Liao, T. Zhou, Q.-J. Yao and B.-F. Shi, *Chem. Commun.*, 2019, **55**, 8514–8523; (*b*) C.-X. Liu, W.-W. Zhang, S.-Y. Yin, Q. Gu and S.-L. You, *J. Am. Chem. Soc.*, 2021, **143**, 14025–14040.

15 Y. Wang, C.-J. Lu, L.-W. Zhan, Y. Wu, J. Feng and R.-R. Liu, *Angew. Chem., Int. Ed.*, 2023, **62**, e202218871.

16 S.-Y. Yin, Q. Zhou, C.-X. Liu, Q. Gu and S.-L. You, *Angew. Chem., Int. Ed.*, 2023, e202305067.

17 For selected reviews, see: (*a*) C. G. Newton, S.-G. Wang, C. C. Oliveira and N. Cramer, *Chem. Rev.*, 2017, **117**, 8908–8976; (*b*) D.-W. Gao, Q. Gu, C. Zheng and S.-L. You, *Acc. Chem. Res.*, 2017, **50**, 351–365; (*c*) A. Link and C. Sparr, *Chem. Soc. Rev.*, 2018, **47**, 3804–3815; (*d*) T. K. Achar, S. Maiti, S. Jana and D. Maiti, *ACS Catal.*, 2020, **10**, 13748–13793; (*e*) J. Wencel-Delord and F. Colobert, *SynOpen*, 2020, **4**, 107–115; (*f*) Q. Zhang, L.-S. Wu and B.-F. Shi, *Chem*, 2022, **8**, 384–413; (*g*) M. I. Lapuh, S. Mazeh and T. Besset, *ACS Catal.*, 2020, **10**, 12898–12919; (*h*) B. Su and J. F. Hartwig, *Angew. Chem., Int. Ed.*, 2022, **61**, e202113343.

18 (*a*) B. Shen, B. Wan and X. Li, *Angew. Chem., Int. Ed.*, 2018, **57**, 15534–15538; (*b*) R. Mi, G. Zheng, Z. Qi and X. Li, *Angew. Chem., Int. Ed.*, 2019, **58**, 17666–17670; (*c*) M. Tian, D. Bai, G. Zheng, J. Chang and X. Li, *J. Am. Chem. Soc.*, 2019, **141**, 9527–9532; (*d*) F. Wang, Z. Qi, Y. Zhao, S. Zhai, G. Zheng, R. Mi, Z. Huang, X. Zhu, X. He and X. Li, *Angew. Chem., Int. Ed.*, 2020, **59**, 13288–13294; (*e*) R. Mi, H. Chen, X. Zhou, N. Li, D. Ji, F. Wang, Y. Lan and X. Li, *Angew. Chem., Int. Ed.*, 2022, **61**, e202111860; (*f*) D. Ji, J. Jing, Y. Wang, Z. Qi, F. Wang, X. Zhang, Y. Wang and X. Li, *Chem*, 2022, **8**, 3346–3362; (*g*) P. Wang, H. Wu, X.-P. Zhang, G. Huang, R. H. Crabtree and X. Li, *J. Am. Chem. Soc.*, 2023, **145**, 8417–8429.

19 (*a*) D. L. Davies, S. M. A. Donald and S. A. Macgregor, *J. Am. Chem. Soc.*, 2005, **127**, 13754–13755; (*b*) M. Lafrance and K. Fagnou, *J. Am. Chem. Soc.*, 2006, **128**, 16496–16497.

20 C. Zheng and S.-L. You, *ACS Catal.*, 2016, **6**, 262–271.

21 Q. Wang, Y.-H. Nie, C.-X. Liu, W.-W. Zhang, Z.-J. Wu, Q. Gu, C. Zheng and S.-L. You, *ACS Catal.*, 2022, **12**, 3083–3093.